

Deep SIMBAD: Active Landmark-based Self-localization Using Ranking -based Scene Descriptor

Tanaka Kanji

Abstract—Landmark-based robot self-localization has recently garnered interest as a highly-compressive domain-invariant approach for performing visual place recognition (VPR) across domains (e.g., time of day, weather, and season). However, landmark-based self-localization can be an ill-posed problem for a passive observer (e.g., manual robot control), as many viewpoints may not provide an effective landmark view. In this study, we consider an active self-localization task by an active observer and present a novel reinforcement learning (RL)-based next-best-view (NBV) planner. Our contributions are as follows. (1) SIMBAD-based VPR: We formulate the problem of landmark-based compact scene description as SIMBAD (similarity-based pattern recognition) and further present its deep learning extension. (2) VPR-to-NBV knowledge transfer: We address the challenge of RL under uncertainty (i.e., active self-localization) by transferring the state recognition ability of VPR to the NBV. (3) NNQL-based NBV: We regard the available VPR as the experience database by adapting nearest-neighbor approximation of Q-learning (NNQL). The result shows an extremely compact data structure that compresses both the VPR and NBV into a single incremental inverted index. Experiments using the public NCLT dataset validated the effectiveness of the proposed approach.

I. INTRODUCTION

Landmark-based robot self-localization has recently garnered interest as a highly-compressive domain-invariant approach for performing visual place recognition (VPR) across domains (e.g., time of day, weather, season). In long-term cross-domain navigation [1]–[3], a robot vision must be able to recognize its location (i.e., self-localization) and the main objects [4] (i.e., landmarks) in the scene. This landmark-based self-localization problem presents two unique challenges. (1) Landmark selection: In the offline training stage, the robot must learn the main landmarks that represent the robot workspace in either a self-supervised or unsupervised manner [5]. (2) Next best view (NBV): In the online self-localization stage, the robot must determine the NBVs to re-identify as many spatially sparse landmarks as possible [6]. This study focuses on the NBV problem.

In landmark-based self-localization, the only available feature (Fig. 1) in each map/live scene x is landmark $p_i (i \in [1, r])$ observed at signal strength $d(x, p_i)$ (i.e., landmark ID + intensity). This is in contrast to many existing self-localization frameworks that assume the availability of vectorial features for each map image. To address this issue, we formulate the landmark-based self-localization as similarity-based pattern recognition (SIMBAD) [7] and present its

deep-learning extension. In pattern recognition, SIMBAD is a highly-compressive method to describe an object as its dissimilarities from r prototypes (e.g., $r = 500$), which is particularly effective when traditional vectorial descriptions of objects are difficult to obtain or inefficient for learning. We adopt SIMBAD because of the following two reasons: (1) First, the landmark selection problem is analogous to and can be informed by the well-investigated problem of prototype selection or optimization [8]. (2) Second, many recent deep learning techniques can effectively measure the (dis)similarity between an object and prototypes [9], instead of directly describing an object. However, the deep learning extension of SIMBAD has not yet been sufficiently investigated, and hence is the main focus of our current study.

Most existing self-localization techniques reported hitherto assume a passive observer (e.g., manual robot control) and do not consider the issue of viewpoint planning or observer control. However, landmark-based self-localization can be an ill-posed problem for a passive observer, as many viewpoints may not provide an effective landmark view. Therefore, we aim to develop an active observer that can adapt its viewpoints, thereby avoiding non-salient scenes that provide no effective landmark view, or moving efficiently toward locations that are the most informative, to reduce sensing/computation costs. This is associated closely with the NBV problem investigated in machine vision studies [10]. However, in our cross-domain scenario, the NBV planner is trained and tested in different domains. The cost for retraining such an NBV planner that does not consider domain shifts is high in cross-domain scenarios, and we intend to address this issue in the current study.



Fig. 1. Motivation. Unlike existing approaches that maintain the model of an entire environment (left panel), we aim to maintain only a small fraction (i.e., landmark regions) of the robot workspace (right panel). Hence, the per-domain cost for retraining (change detection, map updating) is inherently low. However, self-localization with such spatially sparse landmarks can be an ill-posed problem for a passive observer, as many viewpoints may not provide an effective landmark view. Therefore, we considered an active observer and presented an active landmark-based self-localization framework.

Our work has been supported in part by JSPS KAKENHI Grant-in-Aid for Scientific Research (C) 17K00361 and 20K12008.

The authors are with Graduate School of Engineering, University of Fukui, Japan. tnkknj@u-fukui.ac.jp

In this study, we investigated an active landmark-based self-localization framework from a novel perspective of SIMBAD. Our primary contributions are threefold: (1) SIMBAD-based VPR: First, we present a landmark-based compact scene descriptor by introducing a deep-learning extension of SIMBAD. Our strategy is to describe each map/live scene x with dissimilarities $\{d(x, p_i)\}$ from the prototypes (i.e., landmarks) $\{p_i\}_{i=1}^r$ and further compress it into a length h ($\ll r$) list of ranked IDs (e.g., $r = 500$, $h = 4$) of top- h most similar landmarks $\{(v_1, \dots, v_h) | d(x, p_{v_1}) < \dots < d(x, p_{v_h})\}$, which can then be efficiently indexed using an inverted index. (2) VPR-to-NBV knowledge transfer: Second, we address the challenge of RL under uncertainty (i.e., active self-localization) by transferring the state recognition ability of VPR to the NBV. Our scheme is based on a recently developed method of reciprocal rank feature (RRF) [11], inspired by our previous works [11]–[13], which is effective for transfer learning [14] and information retrieval [15]. (3) NNQL-based NBV: Third, we regard the available VPR as the experience database by adapting nearest-neighbor approximation of Q-learning (NNQL) [16]. The result is an extremely compact data structure that compresses the VPR and NBV into a single incremental inverted index. Experiments using the public NCLT dataset validated the effectiveness of the proposed approach.

II. APPROACH

The active self-localization system aims to estimate the robot location on a prelearned route (Fig. 2). It iterates for each viewpoint, three main steps: scene description, (passive) self-localization, and NBV planning. The scene description describes an input map/live image x as its dissimilarities $D(x, \cdot)$ from the predefined landmarks. The (passive) self-localization incorporates each perceptual/action measurement into the belief of the robot viewpoint. The NBV planning takes the scene descriptor x of a live image and determines the NBV action. In addition, three additional

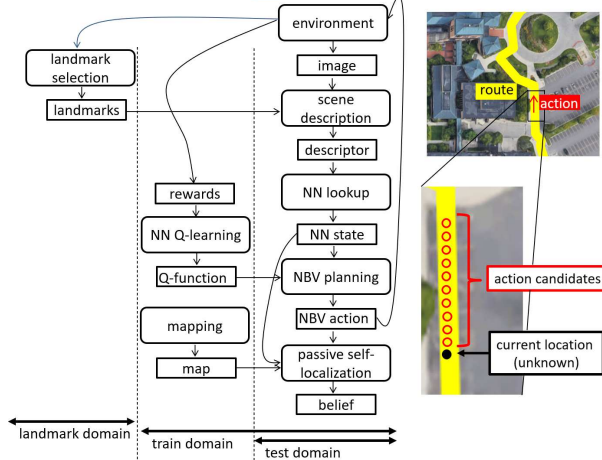


Fig. 2. Active self-localization system. Online processing comprised three main stages: scene description, passive self-localization, and NBV planning. Offline processing comprised landmark selection, mapping, and NN Q-learning. Details of the scene description module are provided in Fig. 3. Details of the NN lookup module are provided in Fig. 4.

modules exist, i.e., landmark selection, mapping, and nearest-neighbor Q-learning, which operates offline to learn the prior knowledge (“landmarks,” “map,” and “Q-function”) required for the abovementioned three main modules. These individual modules are described in detail in the following subsections.

A. Landmark Model

The proposed landmark model can be explained as follows. Let $R = \{p_1, p_2, \dots, p_r\}$ be a set of r predefined prototypes (i.e., landmarks). For a dissimilarity measure d , which measures the dissimilarity between a prototype p and an input object x , one may consider a new description based on the proximities to the set R , as $D(x, R) = [d(x, p_1), d(x, p_2), \dots, d(x, p_r)]$. Here, $D(x, R)$ is a data-dependent mapping $D(\cdot, R): X \rightarrow \mathbb{R}^r$ from a representation X to the dissimilarity space, defined by set R . This is a vector space, in which each dimension corresponds to a dissimilarity $D(\cdot, p_i)$ to the prototype from R . A vector $D(\cdot, p_i)$ of dissimilarities to the prototype p_i can be interpreted as a feature. It is noteworthy that even when no landmark is present in the input image, the proposed model still can describe the image as dissimilarities to the landmarks.

The advantage of this representation is its applicability to any method in dissimilarity spaces, including recent deep learning techniques. For example, d can be (1) a pairwise comparison network (e.g., deep Siamese [17]) that predicts the dissimilarity $d(x, p)$ between p and x , (2) a deep anomaly detection network (e.g., deep autoencoder [18]) that predicts the deviation $d(x|p)$ of x from learned prototypes p , (3) an object proposal network (e.g., feature pyramid network [19]) that predicts object bounding-boxes and class label $d(p|x)$ (e.g., [20]), (4) an L2 distance $|f(x) - f(p)|$ of deep feature $f(\cdot)$ [21] between p and x , as well as (5) any methods for dissimilarities $d(p, x)$ including those for non-visual

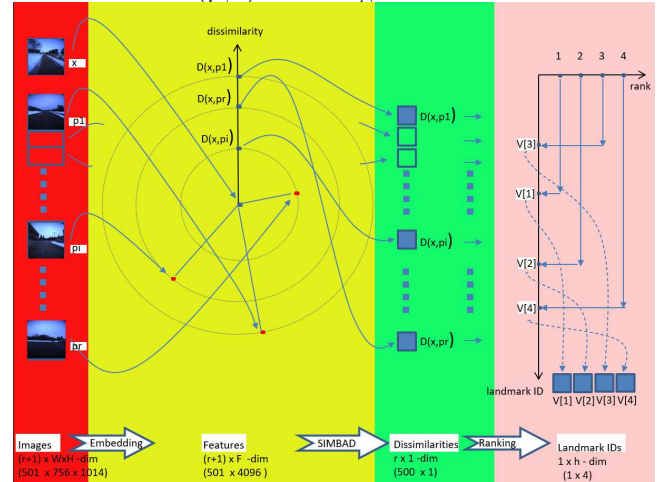


Fig. 3. Scene description module. First, the input query/landmark images are translated into vectorial features. Subsequently, the query feature is described by its dissimilarities from the landmark features. Next, the dissimilarity values are ranked to obtain a ranked list of top- h most similar landmarks. Finally, the proposed landmark ranking-based scene descriptor is obtained.

modalities (e.g., natural language). In the current study, the experimental system was based on (4) using NetVLAD [22] as the feature extraction network $f(\cdot)$. We believe that this enables effective exploitation of the discriminative power of a deep neural network within SIMBAD.

B. Landmark Selection

The landmark selection is performed prior to the training/testing phase, in an independent “landmark domain”. Landmarks should be selected such that they are dissimilar to each other. This is because, if the dissimilarity $d(p_i, p_j)$ is small for a prototype pair, $d(x, p_i) \simeq d(x, p_j)$ for other objects x , then either p_i or p_j is a redundant prototype. Intuitively, an ideal clustering algorithm may identify good landmarks as cluster representatives. However, this clustering is NP-hard [23]. In practice, heuristics such as k-means algorithms are often used as alternatives. Moreover, the utility issue (e.g., [24]) complicates the problem, i.e., landmark visibility and other observation conditions (e.g., occlusions and field-of-views) must be considered to identify useful landmarks. For such landmark selection, only a heuristic approximate solution exists, i.e., no analytical solution exists [5].

In our study, we do not focus on the landmark selection method; instead, we propose a simple and effective method. Our solution comprises three procedures: (1) First, high-dimensional vectorial features $X = \{x\}$ (i.e., NetVLAD) are extracted from individual candidate images. (2) Subsequently, each candidate image $x \in X$ is scored by the dissimilarity $\min_{x' \in X \setminus \{x\}} |x - x'|$ from its nearest neighbor over the other features. (3) Finally, all the candidate images are sorted in the descending order of the scores, and the top- r images are selected as the prototype landmarks. This approach offers two advantages. First, the selected landmarks are expected to be dissimilar to each other. In addition, the dissimilarity features $D(\cdot, R)$ are expected to become accurate when the robot approaches a viewpoint with landmark view.

C. Self-localization

The (offline) mapping is performed prior to the self-localization tasks, in an independent “training domain”. It extracts a 4,096 dim NetVLAD image feature from each map image x and then translates it to an r -dim dissimilarity descriptor $D(x, \cdot)$. Subsequently, it sorts the r elements of the descriptor in the ascending order and returns an ordered list of top- h ranked landmark IDs, which is our proposed h -dim scene descriptor (Fig. 3). With an inverted index, the map image’s ID is indexed by using its landmark ID and the rank value, as primary and secondary keys (Fig. 4).

The (online) self-localization is performed in a new “test domain”. It translates an input query image to a ranking-based descriptor. Subsequently, the inverted index is looked up using each landmark ID in the ordered list as a query. Hence, a short list of map images with a common landmark ID is obtained. Next, the relevance of a map image is evaluated as the inner product $\langle v_{RRF}^r(q), v_{RRF}^h(m) \rangle$ of RRF between the query image q and each map image m in the short list. An RRF v_{RRF}^h is an r -dim h -hot vector whose i -th

element is the reciprocal $1/v[i]$ of the rank value $v[i]$ of the i -th landmark if $v[i] \leq h$, or 0 otherwise. For more details regarding the RRF, please refer to [11].

During the active multi-view self-localization, the results of (passive) self-localization at each viewpoint are incrementally integrated by a particle filter (PF). PF is a computationally efficient implementation of a Bayes filter, and can address multimodal belief distributions [25]. In the PF-based inference system, the robot’s 1D location on the route prelearned in the training domain is regarded as the state. The PF system is initialized at the starting viewpoint of the robot. In the prediction stage, the particles are propagated through a dynamic model using the latest action of the robot. In the update stage, the likelihood models for the landmark observation are approximated by the RRF, and the weight of each k -th particle is updated as $w_k \leftarrow w_k + v_{RRF}[u_k]$, where $v_{RRF}[u_k]$ is the RRF element that corresponds to the hypothesized viewpoint u_k . Other details are the same as that of the PF-based self-localization framework [25].

D. NBV Planning

The NBV planning task is formulated as an RL problem, in which a learning agent interacts with a stochastic environment. The interaction is modeled as a discrete-time discounted Markov decision process (MDP). A discounted MDP is a quintuple (S, A, P, R, γ) , where S and A are the set of states and actions, P the state transition distribution, R the reward function, and $\gamma \in (0, 1)$ a discount factor ($\gamma = 0.9$). We denote by $P(\cdot|s, a)$ and $R(s, a)$ the probability distribution over the next state and the immediate reward of performing action a at state s , respectively.

A Markov policy is the distribution over the control actions for the state, in our case represented by the scene descriptor of a live image (i.e., $s = x$). The action-value function of a policy π , denoted by $Q : S \times A \rightarrow \mathbb{R}$, is defined as the expected sum of discounted rewards that are encountered when policy π is executed. For an MDP, the goal is to identify a policy that yields the best possible values, $Q^*(s, a) = \sup_{\pi} Q^{\pi}(s, a)$, $\forall (s, a) \in S \times A$.

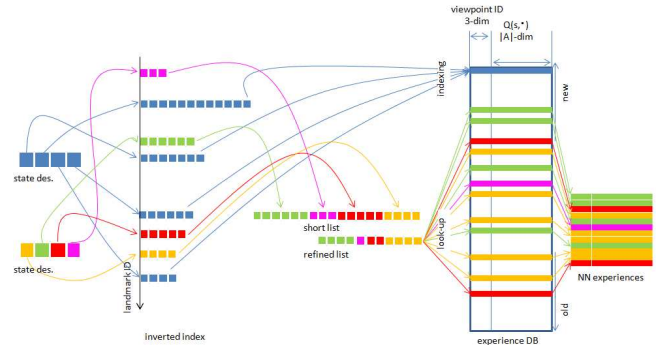


Fig. 4. Nearest neighbor scheme. (1) Offline mapping stage: First, a map image is translated to a landmark ranking-based scene descriptor. Subsequently, the image ID is inserted into the inverted index entries that have common landmark IDs. (2) Online self-localization stage: First, a live image is translated into a landmark ranking-based scene descriptor. Next, a shortlist is obtained from the inverted index entries that have common landmark IDs, and then refined. Finally, the viewpoints or Q-values associated with the nearest neighbor states are obtained from the experience database, and then returned.

The implementation of the “Q-function” $Q(\cdot, \cdot)$ as a computationally tractable function is a key issue. A naive implementation of the function $Q(\cdot, \cdot)$ is to employ a two-dimensional table, which is indexed by a state-action pair (s, a) and whose element is a Q-value [26]. However, this simple implementation presents several limitations. In particular, it requires a significant amount of memory space, proportional to the number and dimensionality of the state vectors, which are intractable in many applications including ours. An alternative approach is to use a deep neural network based approximation of the Q-table (e.g., DQN [27]), as in [28]. However, the DQN must be retrained for every new domain with a significant amount of space/time overhead. Herein, we present a new highly efficient NNQL-based approximation that reuses the existing inverted index (II-C) to approximate $Q(\cdot, \cdot)$ with a small additional space cost.

Our approach is inspired by the recently developed nearest-neighbor approximation of the Q-function (Fig. 4) [16]. Specifically, the inverted index which was originally developed for VPR (II-C) is regarded as a compressed representation of visual experiences in the training domain. Recall that the inverted index aims to index map image ID using the landmark ID. Next, we now introduce a supplementary two-dimensional table called “experience database” that aims to index action-specific Q-values $Q(s, \cdot)$ by map image ID. Subsequently, we approximate the Q-function by the NNQL [16]. The key difference between NNQL and the standard Q-learning is that the Q-value of an input state-action pair (s, a) in the former is approximated by a set of Q-values that are associated with its k nearest neighbors ($k = 4$). Next, we used the supplementary table to store the action-specific Q values $Q(s, \cdot)$. Hence, the Q-function is approximated by $|N(s|a)|^{-1} \sum_{(s', a) \in N(s|a)} Q(s', a)$, where $N(s|a)$ is the nearest neighbor of (s, a) conditioned on a specified action a . In fact, such an action-specific NNQL can be regarded as an instance of RL. For more details regarding NNQL, please refer to [16].

III. EXPERIEMENTS

We evaluated the effectiveness of the proposed algorithm via self-localization tasks in a cross-season scenario.

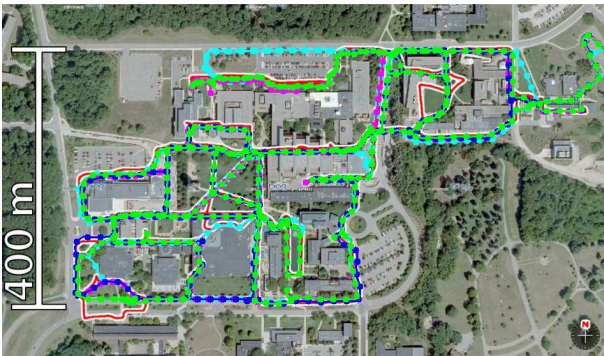


Fig. 5. Experimental environments. The trajectories of the four datasets, “2012/1/22”, “2012/3/31”, “2012/8/4”, and “2012/11/17”, used in our experiments are visualized in green, purple, blue, and light-blue curves, respectively.

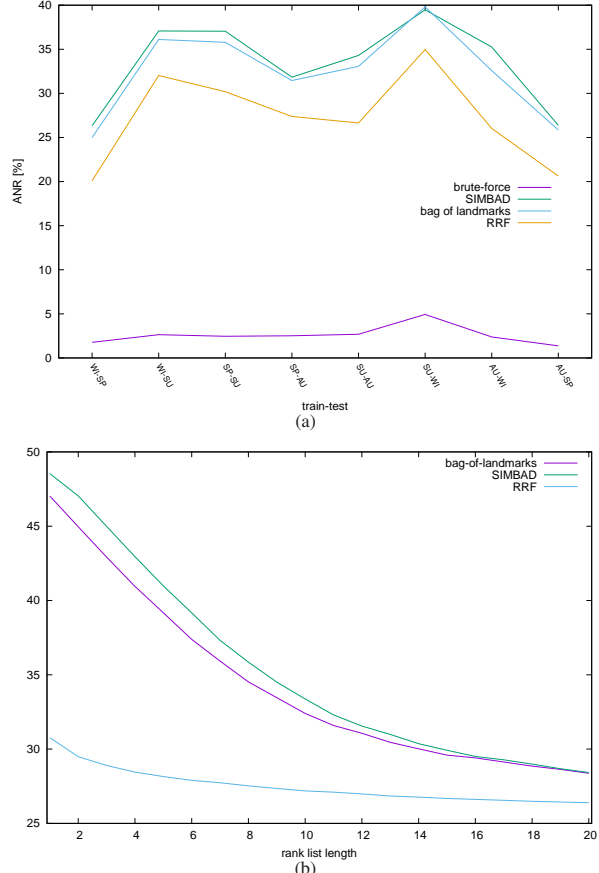


Fig. 6. ANR performance of VPR.

We used the publicly available NCLT dataset [29]. The data we used included view image sequences along vehicle trajectories acquired using the front-facing camera of the Ladybug3, as well as ground-truth GPS viewpoint information. Both indoor and outdoor change objects such as cars, pedestrians, construction machines, posters, and furniture were present during seamless indoor and outdoor navigation by the Segway robot.

In the experiments, we used four different datasets, i.e., “2012/1/22 (WI)”, “2012/3/31 (SP)”, “2012/8/4 (SU)”, and “2012/11/17 (AU)”, which contained 26,208, 26,364, 24,138, and 26,923 images (Fig. 5). They were used to create eight different landmark-training-test domain triplets (Fig. 2): WI-SP-SU, WI-SP-AU, SP-SU-AU, SP-SU-WI, SU-AU-WI, SU-AU-SP, AU-WI-SP, and AU-WI-SU. The number of landmarks was set to 500 for every triplet, which is consistent with the settings in our previous studies using the same dataset (e.g., [30]).

For NNQL training, the learning rate was set $\alpha = 0.1$. Q-value for a state-action pair was initialized to 0.0001, and a positive reward of 100 was assigned when the belief value of the ground-truth viewpoint was top-10% ranked. The number of training episodes was 10,000. The action candidates are a set of forward movements $A = \{1, 2, \dots, 10\}$ [m] along the route defined in the NCLT dataset. One episode consists of an action sequence of length 10, and its starting location is randomly sampled from the route.

The VPR performance at each viewpoint in the context

above was measured based on the averaged normalized rank (ANR). In the ANR, a subjective VPR is modeled as a ranking function that takes an input query image and assigns a rank value to each map image. Subsequently, the rank values for the ground-truth map images are computed, normalized by the number of map images, and averaged over all test queries, thereby yielding the ANR. A VPR system with high ANR performance can be regarded as having nearly perfect performance and high retrieval robustness [31], which is typically required in loop closing applications [32].

Four different scene descriptors based on NetVLAD were developed as the baseline/ablation methods: “brute-force”, “SIMBAD”, “bag-of-(most-similar-)landmarks”, and “RRF”. In “brute-force”, the map model is a nearest-neighbor search based on the L2 dissimilarity measure with NetVLAD of the query image, assuming that every map image is described by the NetVLAD feature. In the other three methods, the map model describes each map image by the dissimilarities with the h most similar landmarks. More specifically, “bag-of-landmarks” assumes h -hot binary (0/1) similarity value, “SIMBAD” uses the h -hot L2 dissimilarity value, and “RRF” uses the h -hot RRF similarity value.

It is noteworthy that the three methods “SIMBAD”, “bag-of-landmarks”, and “RRF” require significantly lower time cost owing to the availability of efficient inverted index.

In terms of space cost, “bag-of-landmarks” is the most efficient, “RRF” and “SIMBAD” are slightly more expensive because they need to memorize the rank value for each map image, and “brute-force” is intractably expensive as it requires to memorize the high-dimensional map features.

Figure 6 shows ANR of single-view VPR tasks.

As can be seen from Fig. 6 (a), the “brute-force” method shows very good recognition performance, but at the cost of high time/space cost for per-domain retraining. As we found in [11], NetVLAD’s utility as a dissimilarity-based feature vector is low. In this experiment, the method “SIMBAD” was about the same as “bag-of-landmarks” and had slightly lower performance. Compared with these two methods, the proposed method “RRF” had much higher performance. To summarize, the proposed method “RRF” achieves a good trade-off between time/space efficiency and recognition performance. In subsequent experiments, we will use this “RRF” as the default method for the passive self-localization module.

As can be seen from Fig. 6 (b), in the case where the rank list length (i.e., descriptor size) is very small (e.g., $h = 4$), the proposed method has a small performance drop, while

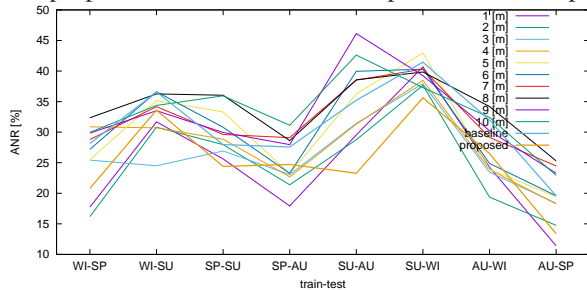


Fig. 7. Performance results for active self-localization.

the other two methods have as bad VPR performance as the chance method (i.e., ANR=50%).

Figure 7 demonstrates the performance of active self-localization. Note that each episode has a different number of valid observations, and long episodes do not always provide high performance. We plot the ANR performance for all test images (frames) on the graph in Fig. 7, regardless of how many episodes were observed. In the figure, “proposed” is the performance of NBV using NNQL trained using the RRF feature as a state vector. “baseline” is different from “proposed” only in that the action is randomly determined. “ $a[m]$ ” ($a \in [1, 10]$) is a naive strategy that repeats the same forward movement $a[m]$ at every viewpoint, independent of the RRFs. They often performed worse than the “proposed”, and to make the matters worse, which action is best is domain-dependent and cannot be known in advance. The characteristics that the higher the VPR performance, the better the active self-localization performance, is consistent with our recent studies dealing with other VPR methods (e.g., pole-landmark-based VPR [28], e.g., convolutional neural network -based VPR [33], and e.g., map-matching-based VPR [34]). It is noteworthy that the proposed method outperformed all the methods considered here, although the landmark-based VPR and NNQL-based NBV were compressed into a single incremental inverted index.

Finally, we also investigated the space/time performance. The inverted index consumes $15h$ -bit per map image. The main processes, extracting NetVLAD features, VPR, and NBV consumes 8.6 ms (GPU), 495.4 ms (CPU), and 7×10^{-3} ms (CPU) per viewpoint (CPU: intel core i3-1115G4 3.00GHz). The most time consuming part is the scene description processing in VPR, which consumes 410 ms. The NBV is significantly fast, compared with the recent deep learning variants, thus the additional cost for the extension from the passive to active self-localization was little.

IV. CONCLUSIONS AND FUTURE DIRECTIONS

Herein, a new framework for active landmark-based self-localization for highly compressive applications (e.g., 40-bit image descriptor) was proposed. Unlike previous approaches of active self-localization, we assumed the main landmark objects as the only available model of the robot’s workspace (“map”), and proposed to describe each map/live scene as dissimilarities to these landmarks. Subsequently, a novel reciprocal rank feature-based VPR-to-NBV knowledge transfer was introduced to address the challenge of RL under uncertainty. Furthermore, an extremely compact data structure that compresses the VPR and NBV into a single incremental inverted index was presented. The proposed framework was experimentally verified using the public NCLT dataset.

Future work must investigate how to accelerate the (dis)similarity evaluator $d(\cdot, \cdot)$ while retaining the ability to discriminate between different levels of (dis)similarities. In the training phase, the evaluator is repeated for every viewpoint of every episode. Since the number of repetitions is very large (e.g., $10,000 \times 10 \times 500 = 5 \times 10^7$), efficiency of calculation is the key to suppress per-domain retraining

cost. Another direction for future research is compression of the proposed scene/state descriptor, towards extremely-compressive applications (e.g., [35]). Although the proposed ranking-based descriptor is the first compact (e.g., 40-bit) descriptor for the VPR-to-NBV applications, it is still uncompressed, i.e., it may be further compressed. Finally, our ongoing research topic is to incorporate various (dis)similarity evaluators into the proposed deep SIMBAD framework, including non-visual -based (dis)similarity evaluators (II-A).

REFERENCES

- [1] M. J. Milford and G. F. Wyeth, "Seqslam: Visual route-based navigation for sunny summer days and stormy winter nights," in *2012 IEEE International Conference on Robotics and Automation*, 2012, pp. 1643–1649.
- [2] W. Churchill and P. Newman, "Experience-based navigation for long-term localisation," *The International Journal of Robotics Research*, vol. 32, no. 14, pp. 1645–1661, 2013.
- [3] R. Arroyo, P. F. Alcantarilla, L. M. Bergasa, and E. Romera, "Fusion and binarization of cnn features for robust topological localization across seasons," in *2016 IEEE/RSJ International Conference on Intelligent Robots and Systems (IROS)*, 2016, pp. 4656–4663.
- [4] A. Torralba, K. P. Murphy, W. T. Freeman, and M. A. Rubin, "Context-based vision system for place and object recognition," in *Computer Vision, IEEE International Conference on*, vol. 2. IEEE Computer Society, 2003, pp. 273–273.
- [5] M. Bürki, C. Cadena, I. Gilitschenski, R. Siegwart, and J. Nieto, "Appearance-based landmark selection for visual localization," *Journal of Field Robotics*, pp. 4137–4143, 2016.
- [6] S. K. Gottipati, K. Seo, D. Bhatt, V. Mai, K. Murthy, and L. Paull, "Deep active localization," *IEEE Robotics and Automation Letters*, vol. 4, no. 4, pp. 4394–4401, 2019.
- [7] A. Feragen, M. Pelillo, and M. Loog, *Similarity-Based Pattern Recognition: Third International Workshop, SIMBAD 2015, Copenhagen, Denmark, October 12-14, 2015. Proceedings*. Springer, 2015, vol. 9370.
- [8] K. S. Gurumoorthy, P. Jawanpuria, and B. Mishra, "Spot: A framework for selection of prototypes using optimal transport," *arXiv preprint arXiv:2103.10159*, 2021.
- [9] B. Li, W. Wu, Q. Wang, F. Zhang, J. Xing, and J. Yan, "Siamrpn++: Evolution of siamese visual tracking with very deep networks," in *Proceedings of the IEEE/CVF Conference on Computer Vision and Pattern Recognition*, 2019, pp. 4282–4291.
- [10] M. Mendoza, J. I. Vazquez-Gomez, H. Taud, L. E. Sucar, and C. Reta, "Supervised learning of the next-best-view for 3d object reconstruction," *Pattern Recognition Letters*, vol. 133, pp. 224–231, 2020.
- [11] K. Takeda and K. Tanaka, "Dark reciprocal-rank: Teacher-to-student knowledge transfer from self-localization model to graph-convolutional neural network," in *2021 International Conference on Robotics and Automation (ICRA)*, 2021, pp. 4348–4355.
- [12] K. Tanaka, "Detection-by-localization: Maintenance-free change object detector," in *2019 International Conference on Robotics and Automation (ICRA)*. IEEE, 2019, pp. 4348–4355.
- [13] —, "Unsupervised part-based scene modeling for visual robot localization," in *2015 IEEE International Conference on Robotics and Automation (ICRA)*. IEEE, 2015, pp. 6359–6365.
- [14] G. Hinton, O. Vinyals, and J. Dean, "Distilling the knowledge in a neural network," *arXiv preprint arXiv:1503.02531*, 2015.
- [15] P. K. Atrey, M. A. Hossain, A. El Saddik, and M. S. Kankanhalli, "Multimodal fusion for multimedia analysis: a survey," *Multimedia systems*, vol. 16, no. 6, pp. 345–379, 2010.
- [16] D. Shah and Q. Xie, "Q-learning with nearest neighbors," *arXiv preprint arXiv:1802.03900*, 2018.
- [17] Y. Zhan, K. Fu, M. Yan, X. Sun, H. Wang, and X. Qiu, "Change detection based on deep siamese convolutional network for optical aerial images," *IEEE Geoscience and Remote Sensing Letters*, vol. 14, no. 10, pp. 1845–1849, 2017.
- [18] J. An and S. Cho, "Variational autoencoder based anomaly detection using reconstruction probability," *Special Lecture on IE*, vol. 2, no. 1, pp. 1–18, 2015.
- [19] S.-W. Kim, H.-K. Kook, J.-Y. Sun, M.-C. Kang, and S.-J. Ko, "Parallel feature pyramid network for object detection," in *Proceedings of the European Conference on Computer Vision (ECCV)*, 2018, pp. 234–250.
- [20] S. Hanada and K. Tanaka, "Partslam: Unsupervised part-based scene modeling for fast succinct map matching," in *2013 IEEE/RSJ International Conference on Intelligent Robots and Systems*. IEEE, 2013, pp. 1582–1588.
- [21] A. Babenko, A. Slesarev, A. Chigorin, and V. Lempitsky, "Neural codes for image retrieval," in *European conference on computer vision*. Springer, 2014, pp. 584–599.
- [22] R. Arandjelovic, P. Gronat, A. Torii, T. Pajdla, and J. Sivic, "Netvlad: Cnn architecture for weakly supervised place recognition," pp. 5297–5307, 2016.
- [23] K. Tanaka, "Self-supervised map-segmentation by mining minimal-map-segments," in *2020 IEEE Intelligent Vehicles Symposium (IV)*. IEEE, 2020, pp. 637–644.
- [24] K. Tanaka, H. Zha, and T. Hasegawa, "Viewpoint planning in map updating task for improving utility of a map," in *Proceedings 2003 IEEE/RSJ International Conference on Intelligent Robots and Systems (IROS 2003)(Cat. No. 03CH37453)*, vol. 1. IEEE, 2003, pp. 729–734.
- [25] F. Dellaert, D. Fox, W. Burgard, and S. Thrun, "Monte carlo localization for mobile robots," in *1999 International Conference on Robotics and Automation (ICRA)*, vol. 2, 1999, pp. 1322–1328.
- [26] R. S. Sutton, A. G. Barto, et al., *Introduction to reinforcement learning*. MIT press Cambridge, 1998, vol. 135.
- [27] J. Fan, Z. Wang, Y. Xie, and Z. Yang, "A theoretical analysis of deep q-learning," in *Learning for Dynamics and Control*. PMLR, 2020, pp. 486–489.
- [28] K. Tanaka, "Active cross-domain self-localization using pole-like landmarks," in *2021 IEEE International Conference on Mechatronics and Automation (ICMA)*, 2021, pp. 1188–1194.
- [29] N. Carlevaris-Bianco, A. K. Ushani, and R. M. Eustice, "University of michigan north campus long-term vision and lidar dataset," *The International Journal of Robotics Research*, vol. 35, no. 9, pp. 1023–1035, 2016.
- [30] T. Hiroki and K. Tanaka, "Long-term knowledge distillation of visual place classifiers," in *2019 22st International Conference on Intelligent Transportation Systems (ITSC)*, 2019.
- [31] P. Hiremath and J. Pujari, "Content based image retrieval using color, texture and shape features," in *15th International Conference on Advanced Computing and Communications (ADCOM 2007)*. IEEE, 2007, pp. 780–784.
- [32] J. P. Company-Corcoles, E. Garcia-Fidalgo, and A. Ortiz, "Lipolcd: Combining lines and points for appearance-based loop closure detection," in *BMVC*, 2020.
- [33] K. Kurauchi and K. Tanaka, "Deep next-best-view planner for cross-season visual route classification," in *2020 25th International Conference on Pattern Recognition (ICPR)*, 2021, pp. 497–502.
- [34] K. Tanaka, "Active map-matching: Teacher-to-student knowledge transfer from visual-place-recognition model to next-best-view planner for active cross-domain self-localization," in *2021 IEEE International Conference on Computational Intelligence and Virtual Environments for Measurement Systems and Applications (CIVEMSA)*, 2021, pp. 1–6.
- [35] F. Yan, O. Vysotska, and C. Stachniss, "Global localization on openstreetmap using 4-bit semantic descriptors," in *2019 European Conference on Mobile Robots (ECMR)*. IEEE, 2019, pp. 1–7.